A high-performance, bifunctional oxygen electrode catalysed with palladium and nickel-iron hexacyanoferrate

R.D. McKerracher [a], H.A. Figueredo-Rodríguez, [a] C. Ponce de León [a,*], C. Alegre [b], V. Baglio [b], A.S. Aricò [b], F.C. Walsh [a]

[a]Electrochemical Engineering Laboratory, Engineering Sciences, Faculty of Engineering and the Environment, University of Southampton, Highfield, Southampton, SO17 1BJ, UK

[b]Consiglio Nazionale delle Ricerche, Istituto di Tecnologie Avanzate per l'Energia " Nicola Giordano", Salita S.Lucia sopra Contesse, 5. 98126 Messina, Italy

Abstract

The development of air-breathing cathodes, which utilise atmospheric oxygen, enables the construction of lightweight, high energy density metal-air batteries and fuel cells. Air electrodes can be very lightweight and thin because the active material, oxygen, does not need to be stored inside the cell. However, air electrodes are restricted by poor reaction kinetics and low activity of many catalysts towards the oxygen evolution and reduction reactions. In addition, it is a challenge to maintain chemical and mechanical stability of the catalyst and supporting materials at oxidising currents under the strong alkaline conditions commonly used, and gas evolution. This paper reports a novel bifunctional oxygen electrode with remarkable stability, able to perform at current densities up to 1,000 mA cm^{-2} and withstand 3,000 cycles continuously. The electrode is catalysed by a mixture of Pd/C and mixed nickel-iron hexocyanoferrate, which have high activities towards the ORR and OER reactions, respectively.

Key words: air cathode; bifunctional electrode; metal air batteries; nickel-iron; palladium.

1. **Introduction**

Metal/air batteries (MABs) use oxygen from the atmosphere, in contrast to traditional batteries where the reagents are contained within the cell. Several systems for fundamental studies or as prototypes exist but only few have reached commercial stage. Typical MABs include Zn/O_2,[1] Li/O_2,[2] Na/O_2, [3] K/O_2,[4] Mg/O_2,[5] Ca/O_2,[6] Al/O_2,[7] Si/O_2,[8] and Fe/O_2 [9]. In non-aqueous systems during the discharge cycle, the metal oxidises and its ions migrate through the electrolyte to the gas diffusion electrode (GDE) where they form a solid oxide with the reduced oxygen. Similar processes occur in aqueous systems, in some cases, the oxide forms on the metal electrode such as in the iron–air battery, where the formation of the solids $Fe(OH)_2$ and Fe_3O_4 occurs [10]. In other cases such as in the zinc–air battery, zincate ion $Zn(OH)_4^-$ ions dissolve in the strong alkaline electrolyte. In non-rechargeable batteries, the metal oxide is stable and the capacity of the battery depends on the amount of metal; the battery is recycled once the metal is consumed. Recently, there has been an increased interest in rechargeable metal-air batteries. In non-aqueous systems, the battery is recharged by electrodeposition of metal at the negative electrode together with the oxygen evolution from the oxide decomposition at the positive electrode, while in aqueous systems, the battery is charged by the electrodeposition of metal at the negative electrode together with oxygen evolution reaction (OER) via the oxidation of water, at the positive electrode.

In aqueous systems the oxygen reduction reaction (ORR) and the oxygen evolution reaction (OER) occur on the same electrode during the discharge and charge cycles, respectively. This requires a special bifunctional catalyst. Ideally, this catalyst should be able to facilitate both reactions close to the equilibrium potential. One of the main challenges of designing a bifunctional oxygen electrode is producing an electrochemically stable catalyst which is highly

active towards both the ORR and OER, and is supported within a stable high surface area catalyst layer. Carbon is a popular choice for a catalyst support but it has proven a challenge to maintain its mechanical and electrochemical stability during repeated charge-discharge cycles [11, 12]. Therefore, even if the catalyst is highly effective, the catalyst layer of the electrode may degrade or disintegrate during oxygen evolution. This can be minimised by using highly graphitised carbons that are more corrosion resistant. Since the oxygen reduction and evolution reactions occur at the point of contact between the electrolyte and the catalyst, the catalyst support requires a highly porous structure in order to allow the oxygen gas to enter and exit the structure easily. It is also desirable that the morphology of the electrode surface is designed in such a way that facilitates the rapid formation and removal of the gas bubbles. However, a compromise should be made to provide the highly porous structure required with the mechanical stability of the electrode.

Commercially available oxygen electrodes have various geometrical characteristics: electrodes that favour the OER allow the oxygen bubbles to escape through open structures such as open meshes or tilted structures. Electrodes for the ORR use highly porous surface structures (35% – 65%) rigid carbon supports and a gas diffusion layer (GDL) with modulated porosity (100– 300 microns) with the catalytic layer on top (2–1000 nm thickness). Since the two oxygen reactions require different electrode characteristics, a compromise between structure types is required to maximise the bifunctional activity and stability of the catalyst. The electrode should facilitate the release of oxygen generated during the charge cycle whilst allowing oxygen from the air to enter during the discharge cycle. While most laboratory studies use pure oxygen to evaluate the electrodes, metal-air batteries should be able to work with atmospheric air which will require a larger flow rate to compensate for the ca. 21 % oxygen content of air. Experiments with oxygen help to determine the catalyst activity but might mask the true effects

of mass transport when air is used. In this paper, pure oxygen was used to evaluate the catalytic activity of the electrodes, in order that the results are standardised (the oxygen content of air will vary in different laboratories; whereas pure oxygen from a cylinder is always 100% oxygen).

Typical bifunctional catalysts used in oxygen electrodes include platinum [13] palladium [9] and non-noble metal compound phases, such as perovskites, [14] spinels, [15, 16] and pyrochlores [17]. Perovskite catalysts mixed with high surface area carbon are some of the most promising bifunctional catalyst materials produced to date but reported data varies depending on the type of perovskite and operational conditions. Velraj et al. [18] reported that the performance of electrodes prepared with perovskite catalyst ($La_{0.6}Ca_{0.4}CoO_3$ or $Sr_{0.5}Sm_{0.5}CoO_{3-\delta}$) with different Vulcan XC-72R carbon black at ±50 mA cm^{-2} (OER and ORR at +0.65 V and -0.2 V vs. Hg/HgO, respectively) in 8.5 mol dm^{-3} KOH, was limited to 100-110 cycles due to degradation of the carbon support. The catalyst maintained its catalytic activity and the authors suggested that alternative non-carbon supports need to be developed, such as Nb-doped TiO_2 nanoparticles [19] or Ebonex [20]. Gas diffusion electrodes manufactured with perovskite catalysts of type $La_{0.6}Ca_{0.4}Co_{0.8}B_{0.2}O_3$ (B = Mn, Fe, Co, Ni, Cu) developed by Shimizu et al. [21] in 7 mol dm^{-3} KOH reached up to 240 cycles at ±100 mA cm^2 (OER and ORR at +0.6 V and -0.4 V vs. Hg/HgO, respectively).

Recently, a bifunctional palladium-based catalyst was produced on a carbon support with exceptionally good corrosion resistance compared with those used in commercial Pt electrodes, [9] circumventing some of the degradation problems associated with repeated cycling of bifunctional oxygen electrodes in alkaline solution. The loading of palladium on this electrode

was only 0.5 mg cm^{-2}, four times lower than a commercial Pt/C electrode. This electrode achieved a stable oxygen evolution potential over 1,000 charge-discharge cycles, and had +0.01 and +0.54 V vs. Hg/HgO onset potentials for oxygen reduction and evolution respectively.

This paper reports the manufacture and performance of a highly stable novel air-breathing electrode which contains a mixture of the Pd/C catalyst materials reported previously [9] with a newly-developed low-cost oxygen catalyst based on a mixed Ni/Fe hexacyanoferrate (referred to as the "Ni/Fe catalyst" in this publication). The performance of the catalysts was complimentary as the Pd/C catalyst had high activity towards the ORR, and the Ni/Fe catalyst had high activity towards the OER. The catalyst materials were first tested on a RDE, and then included in the catalyst layer of a GDE electrode to provide valuable information on catalyst performance that could be used during the scale-up process.

2. Experimental

2.1. Synthesis of Ni/Fe hexacyanoferrate catalyst (for OER)

A 50 cm^3 aqueous solution containing 0.12 mol dm^{-3} NiSO$_4$.6H$_2$O and 0.03 mol dm^{-3} FeSO$_4$.7H$_2$O was added to a 50 cm^3 solution of 0.1 mol dm^{-3} K$_3$[Fe(CN)$_6$] and left stirring overnight at 1200 rpm and 20 ^{o}C. The solution was centrifuged to separate the Ni/Fe catalyst which was dried at 60℃ for 24 hours.

2.2. Synthesis of Pd/C catalyst (for ORR)

The Pd/C catalyst was synthesized by a colloidal method, employing sulphites as complexing agents, as described elsewhere [22, 23]. The carbon support (supplied by IMERYS Graphite & Carbon, 220 m^{2}g^{-1} surface area) was suspended in distilled water and stirred in an ultrasonic

water bath at 80 °C to form a slurry. An acidic solution containing an appropriate amount (to reach a final loading of 30 wt. % of Pd on the support) of $Na_6Pd(SO_3)_4$ was successively added to the slurry. The Pd sulphite complex solution was decomposed by adding H_2O_2 and successively increasing the pH to 5.5 to form colloidal PdO_x/C. The metallic oxide was reduced in a H_2 stream at room temperature (23 °C) to form the 30 wt. % Pd/C catalyst.

2.3. Construction of the gas diffusion electrodes

The gas diffusion electrode was produced using a similar method to that reported in a previous publication. [9] A 50 × 50 x 0.11 mm piece of 25 wt. % PTFE-treated carbon cloth (FuelCell.com), was coated with a 100 μm layer of a paste containing 80 wt. % carbon (64 m^2 g^{-1}, IMERYS) and 20 wt. % PTFE (DISP 30 solution, DuPont) to form the gas diffusion layer (GDL) [2].

For the mixed-catalyst electrode, the catalyst layer was an ink made from 42 mg 30 wt. % Pd/C and 125 mg Ni/Fe with 25 mg carbon, the mixture being sonicated for 15 minutes in a 5 wt. % Nafion® aliphatic alcohol suspension (Sigma Aldrich), with a 3:2 weight ratio of (catalysts + carbon):Nafion. This provided a 5 mg cm^{-2} Ni/Fe loading and a 0.5 mg cm^{-2} Pd loading. A 0.05 mm thick nickel mesh (Dexmet, 32) current collector was placed above the catalyst layer and the electrode was pressed for 2 minutes at 180 ˚C at 5 MPa (Carver, model 3851 press).

As well as the mixed catalyst electrode, two electrodes were produced that contained only one of the catalysts; 5 mg cm^{-2} Ni/Fe or 0.5 mg cm^{-2} Pd/C, in the same mass quantities as shown above.

2.4. Characterisation of the catalysts

Scanning electron microscopy (SEM) was performed on a 0.5-30 kV JSM 6500F thermal emission SEM. Transmission electron microscopy (TEM) was performed using a 300 kV JEOL 3010 TEM on S147-3 copper grids coated with perforated carbon film (Agar Scientific). Infrared spectroscopy was performed on a Nicolet iS10 spectrometer (Thermo Fisher Scientific).

2.5. Electrochemical analysis

For the electrochemical analysis, the GDE was clamped onto a flange of a 3-electrode cell, exposing a 0.785 cm^2 circular area to a 6 mol dm^{-3} KOH electrolyte. The counter electrode was a 1 cm^2 platinum mesh and the reference electrode was a Hg/HgO (1 mol dm^{-3} KOH) electrode (Hach-Lange, - 0.115 V *vs.* SHE). Oxygen gas (99.999 % purity, BOC) was circulated at atmospheric pressure via a glass tap in the back at a rate of 100 cm^3 min^{-1}. Cyclic voltammograms (CVs) at 1 mV s^{-1}, and charge-discharge profiles at constant current, were recorded using a potentiostat (Metrohm PGSTAT 302N). The cell was fitted with a glass jacket to circulate water from a water bath at a controlled temperature 0-100 ˚C (Julabo, model F12-EH). The reference and counter electrodes were the same as used for the RDE experiments. A fresh piece of GDE was used for each scan or each series of charge-discharge cycles.

3. Results and Discussion

3.1. Characterisation of the gas diffusion electrodes

The SEM images in Figure 1 show the cross-sectional structure of the gas diffusion electrodes catalysed with Pd/C and Ni/Fe catalysts. The electrodes, produced via a hot-pressing method, were approximately 0.5 mm thick, and had a three-layered structure of gas diffusion layer, catalyst layer and nickel current collector. In these images, the uncut side of the electrode that had not been subject to any forces other than the original hot-pressing was presented to the

electrode beam. The layers were mutually adherent with a dense layer of compacted powder within the catalyst layer. The total thickness was regular and consistent along the length of the electrode, although the thickness of the gas diffusion layer varied slightly owing to the irregular shape of the carbon cloth fibres, meaning that in some areas the overlaying catalyst layer is more compressed than in others.

TEM and XRD investigations of the catalyst particles revealed that the Pd/C catalyst has a Pd a crystallite size of ca. 10.0 nm, and the Pd shows a typical face centered cubic structure (fcc), as reported previously [9]. The Pd particles were well-dispersed on the carbon support (Figure 2a), and the carbon support particles had a partially graphitic structure, which is required for withstanding oxidizing potentials. Thermal gravimetric analysis confirmed the metal concentration of 30 wt. % Pd with an estimated accuracy of ±1% [9].

The Ni/Fe hexacyanoferrate particles were larger (Figure 2b), with 20-30 nm agglomerated particles. The crystalline XRD pattern (Figure 3a) can be indexed with reflections similar to $Ni_3[Fe(CN)_6]_2$ [24]. Elemental analysis of a 100 μm^2 aggregate using SEM (Figure 3b) showed an atomic ratio of 1:1 Ni:Fe. The FTIR spectrum (Figure 3c) shows a structure similar to $Ni_3[Fe(CN)_6]_2$ and $Fe_3[Fe(CN)_6]_2$, with CN stretching modes at 2047 and 2165 cm^{-1} [25, 26]. The 3306 cm^{-1} and 1603cm^{-1} peaks indicate crystallographic water, [26, 27] and C-O stretching peaks at 1120 and 1030 cm^{-1} suggest carbonates chemisorbed on the surface [28]. The 592 cm^{-1} peak is due to Fe-CN bending [25]. The XRD, EDX and FTIR results combined suggest a hybrid structure of $Ni_3[Fe(CN)_6]_2$ and $Fe_3[Fe(CN)_6]_2$, with molecular formula $Ni_5Fe[Fe(CN)_6]_4$.

3.2. *Electrochemical analysis of the mixed catalyst oxygen electrode*

The gas diffusion electrodes were examined in a 3-electrode glass cell to compare the behaviour of a mixed catalyst Ni/Fe + Pd electrode with that of electrodes only containing a single catalyst. Figure 4 shows cyclic voltammetry of the electrodes containing Pd, Ni/Fe and Ni/Fe + Pd catalysts. The behaviour of the mixed catalyst electrode is very interesting compared to the electrodes that used the catalysts separately. The curves show that for the oxygen reduction reaction, the electrode performance in terms of reduction onset potential and current density at the Ni/Fe + Pd is very similar to that of the Pd electrode, since Pd is a superior ORR catalyst to Ni/Fe [29]. For the OER, the performance of the mixed catalyst electrode did not equal that of the Ni/Fe catalyst. In fact, there seems to be an additive effect where the presence of both catalysts enhances the OER performance. The onset potential for the OER is the same for Ni/Fe + Pd as Ni/Fe, at +0.33 V *vs.* Hg/HgO, but the current density is twice as high at +0.65 V *vs.* Hg/HgO for the Ni/Fe + Pd electrode. The current density at the Ni/Fe + Pd electrode at this potential is greater than the sum of the current density at Ni/Fe and Pd electrodes possibly due to a higher porous structure. Also, the reaction between Pd and Ni/Fe at high positive potentials in the mixed electrode that enhances the rate of oxygen evolution also might enhance the electrical conductivity of the Ni/Fe hexacyanoferrate (hexacyanoferrate has a low conductivity whereas Pd is metallic).

The charge-discharge profiles of the electrodes were compared at 20 mA cm^{-2} in 6 mol dm^{-3} KOH over 4 days, with 4 hours for each cycle. All of the electrodes were stable over the cycling period, but those electrodes containing the Ni/Fe catalyst showed the best stability and performance during the OER (charging cycle). The stability of the potential during each cycle was poorer with the Pd catalysed electrode. For example, in several cycles the potential curve did not reach a level current, suggesting that some corrosion may be occurring. For the OER,

the presence of Pd in the mixed Ni/Fe + Pd air electrode did not seem to adversely affect its performance compared with the electrode catalysed by Ni/Fe alone. For the ORR, the Ni/Fe+Pd electrode showed the lowest overpotentials, and the performance of the all the electrodes appeared to stabilise after 25 hours cycling.

The charge-discharge cycles in Figure 5 appeared to show the opposite behaviour to the cyclic voltammetry, as the combination of catalysts Ni/Fe + Pd improved the ORR performance more than the OER performance. Charge-discharge profiles often show different behaviour to the cyclic voltammetry, i.e. during cyclic voltammetry, the potential is only held at a certain value for a few miliseconds or seconds, whereas during charge-discharge cycling the constant current drives a strong overpotential for several hours. It may be that the OER is more sensitive to the effect of being held at high potentials for extended period of time than the ORR, particularly as most of the adverse reactions such as carbon corrosion occur at positive, rather than negative, potentials [30, 31].

The cyclic voltammetry was compared to voltammograms recorded in other publications in similar conditions for other gas diffusion air electrodes [32, 33, 34, 35, 36]. Figure 6 shows the data for two scans of the Ni/Fe + Pd air electrode, from the equilibrium potential (where $j = 0$) of +0.33 V $vs.$ Hg/HgO, in the negative potential direction (ORR) and the positive direction (OER), compared with data from the literature. The peak at c.a. +0.45 V $vs.$ Hg/HgO is caused by nickel oxidation [37] and slightly masks the onset of oxygen evolution, which begins at +0.33 V $vs.$ Hg/HgO. For the OER, the Ni/Fe + Pd air electrode outperforms all the other air electrodes in terms of current density. For the ORR, it appears that some of the Pt/C electrodes and perovskite electrodes reported in the literature generate a higher current density and have lower ORR onset overpotentials than the Ni/Fe+Pd air electrode, [32, 33] but these electrodes

did not show such good OER current densities or onset potentials. On balance, the Ni/Fe + Pd air electrode shows the strongest bifunctional oxygen performance.

The Ni/Fe + Pd electrode was systematically cycled at different current densities to analyse its performance limits. Figures 7 and 8 show how the charge and discharge potentials at the air electrode vary with cycles of increasing current density. The electrode showed stability over a wide range of current densities, which is unusual for a carbon-based gas diffusion electrode [12]. In Figure 8, the current densities of the charge-discharge cycle were progressively increased above 200 mA cm^{-2} and the electrode did not show significant signs of instability in the potential until 1000 mA cm^{-2}. The electrode was cycled up to 2000 mA cm^{-2} then cycled at 300 mA cm^{-2} (Figure 6) to see if the electrode was still functional. In fact, the performance of the electrode was still quite similar to the previous cycle at 300 mA cm^{-2}, even though it had been subjected to high current densities. The overpotentials of the OER and ORR had increased, however, and the ORR potential was unstable (see the final cycle in Figure 8).

The relationship between potential reached by the Ni/Fe + Pd electrode during charging/ discharging and the current density is plotted in Figure 9 with the same relationship shown for the Pd electrode and also for a commercial Pt/C air electrode produced by Gaskatel (using data obtained in a previous publication) [9]. It is clear that both the Pt and Pd catalysed electrodes suffered a deterioration in potential at a lower current density than the Ni/Fe+Pd electrode. At lower current density (<20 mA cm^{-2}) the commercial Pt/C electrode showed a better performance for the OER than the other two electrodes but this effect did not persist in a higher current density range. It was previously shown that the stability of the commercial Pt/C in strongly alkaline 6 mol dm^{-3} KOH solution was much lower over several days cycling [9]. It should be noted that this electrode is not a bifunctional electrode and was not designed to

operate in strong alkaline environments, so its stability was not expected to be very high. It is, however, a useful guide to compare the results of the Ni/Fe+Pd electrode catalyst at short periods of time.

Finally, the effect of thousands of multiple rapid cycles was also examined at 80 and 150 mA cm^{-2} current density. Figure 10 shows 3,000 charge-discharge cycles of 2 minutes each (the ORR and OER plateaus appear as continuous line because the cycles were so short). Cycling the electrodes many times at increasingly higher current densities is a useful technique for estimating within a short time period how the air electrode may perform after many charge discharge cycles at a lower current density with a much longer duration (i.e. several hours). The Ni/Fe+Pd air electrode appears to reach a stable potential within 1 hour, and only show a small deterioration in performance after this time. The OER and ORR overpotentials are slightly larger than would be expected at these current densities from Figure 9 but this may be a reflection of the extreme conditions (rapid charge-discharge cycling 60 times per hour) that have increased the rate of carbon and catalyst corrosion at the electrode.

4. Conclusions

A bifunctional oxygen electrode was successfully manufactured using a mixture of 30 wt. % Pd on carbon (0.5. mg cm^{-2} loading) and Ni/Fe hexacyanoferrate (5 mg cm^{-2} loading), on a carbon based gas-diffusion electrode showing good corrosion resistance. The mixed catalyst electrode showed lower overpotentials and higher current densities for oxygen evolution and reduction compared with the individual Pd and Ni/Fe catalysts. Although the Pt/C commercial electrode is not designed as a bifunctional electrode, the mixed catalyst electrode outperformed it over the entire current density range over short periods of time. The loading of the Pd precious metal was kept very low (four times less than the commercial electrode) to reduce the cost of

the air electrode, with a higher loading of the low-cost Ni/Fe catalyst being used to enhance the electrode performance.

The oxygen reduction onset potential at the Ni/Fe+Pd electrode was -0.05 V *vs*. Hg/HgO and the oxygen evolution onset potential was +0.33 V *vs*. Hg/HgO, and at 20 mA cm^{-2} charging and discharging current the electrode achieved stable potentials at -0.14 and +0.53 V *vs*. Hg/HgO, respectively. The electrode was functional at up to 1,000 mA cm^{-2} current density and could be cycled 3,000 times at high current density (150 mA cm^{-2}), without significant increases in the oxygen reduction and evolution overpotentials.

Acknowledgements

Figure captions

Figure 1   Scanning electron microscopy images showing side view cross-sections of gas-diffusion oxygen electrode catalysed by (a) Pd/C (b) Ni/Fe and (c) Pd/C + Ni/Fe mixture.

Figure 2.   Transmission electrode microscopy images of the catalysts (a) Pd/C and (b) Ni/Fe.

Figure 3.   (a) Powder XRD pattern of the Ni/Fe catalyst, (b) EDX elemental analysis of a Ni/Fe particle aggregate and (c) FTIR spectrum of 10 mg of Ni/Fe catalyst powder.

Figure 4.   Cyclic voltammograms of gas diffusion air electrodes at 1 mV s^{-1} in 6 mol dm^{-3} KOH, with 100 mL min^{-1} O$_2$ flow into the back of the electrodes. The labels Pd, Ni/Fe and Ni/Fe + Pd denote the catalysts used.

Figure 5.   Charge discharge profiles of gas diffusion air electrodes at 20 mA cm^{-2} in 6 mol dm^{-3} KOH, with 100 ml min^{-1} O$_2$ flow into the back of the electrodes. The labels Pd, Ni/Fe and Ni/Fe + Pd denote the catalysts used.

Figure 6.   Cyclic voltammograms of the Ni/Fe + Pd gas diffusion air electrode at 1 mV s^{-1} in 6 mol dm^{-3} KOH, with 100 ml min^{-1} O$_2$ flow into the back of the electrodes, compared with data from gas diffusion electrodes in the literature catalysed by Ag nanoparticles (NP) [36] LaMnO$_3$ [35] LaMnO$_3$ (2) [34] LCCO perovskite [33], Pt/C JM (JM = Johnson Matthey) [32] Pt/C (Gaskatel GmbH) [9].

Figure 7.   Charge discharge profiles of the Ni/Fe + Pd catalysed gas diffusion air electrodes at 40 – 200 mA cm^{-2} current density in 6 mol dm^{-3} KOH, with 100 ml min^{-1} O$_2$ flow into the back of the electrodes.

Figure 8.   Charge discharge profiles of the Ni/Fe + Pd catalysed gas diffusion air electrodes at a current density of 300 – 2000 mA cm^{-2} current density in 6 mol dm^{-3} KOH, with 100 ml min^{-1} O$_2$ flow into the back of the electrodes.

Figure 9.   Variation of air electrode charge and discharge potential with increasing current density for Ni/Fe + Pd, Pd, and commercial Pt/C air electrodes (Gaskatel).

Figure 10.   Charge-discharge cycles of Pd + Ni/Fe catalysed air electrode with cycles at 80 and 150 mA cm^{-2} current density, over 3,000 cycles of 2 minutes each (1 minute charge, 1 minute discharge).
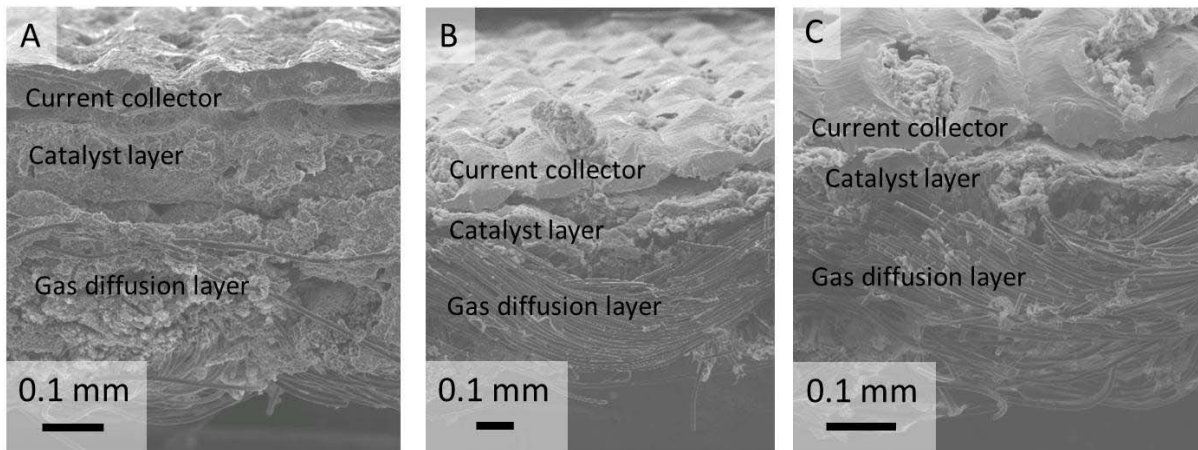
Figures

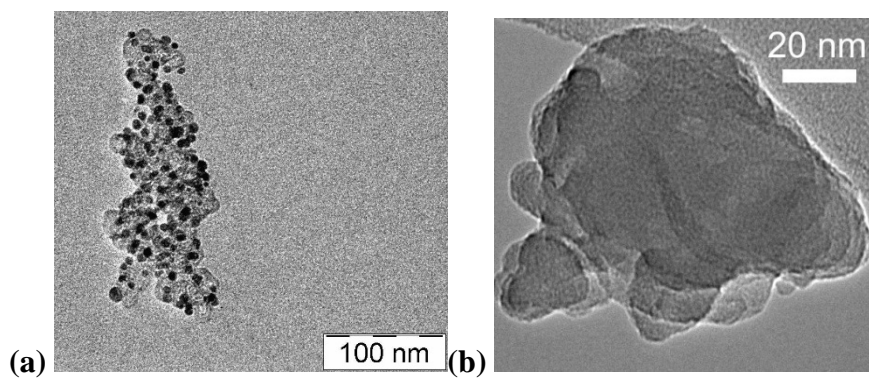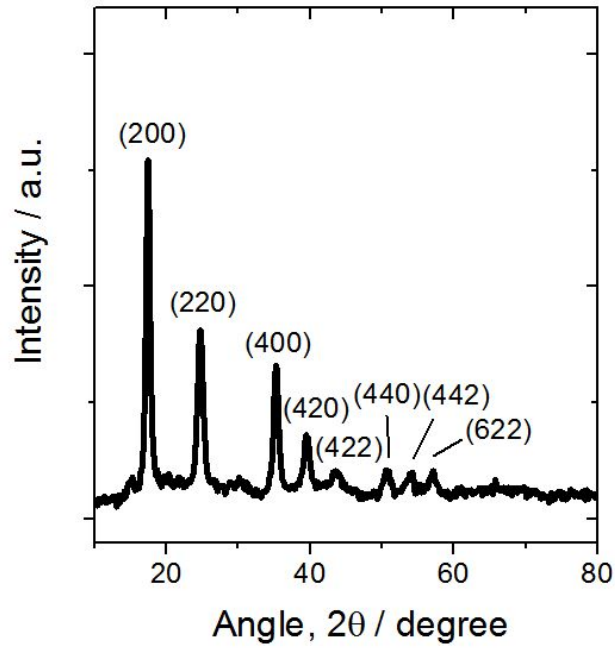
Figure 1

Figure 2

Figure 3a
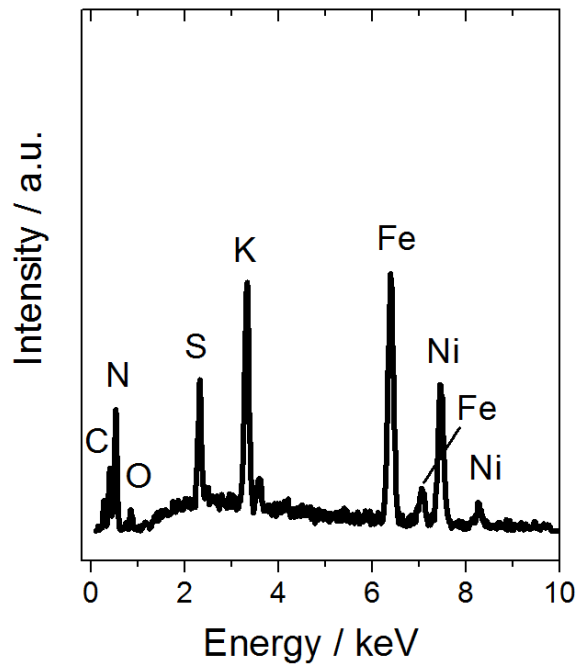
Figure 3b
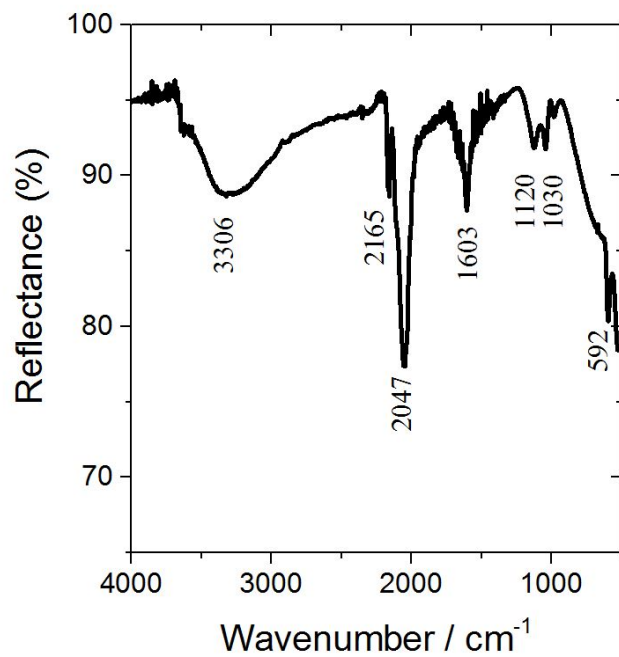
Figure 3c
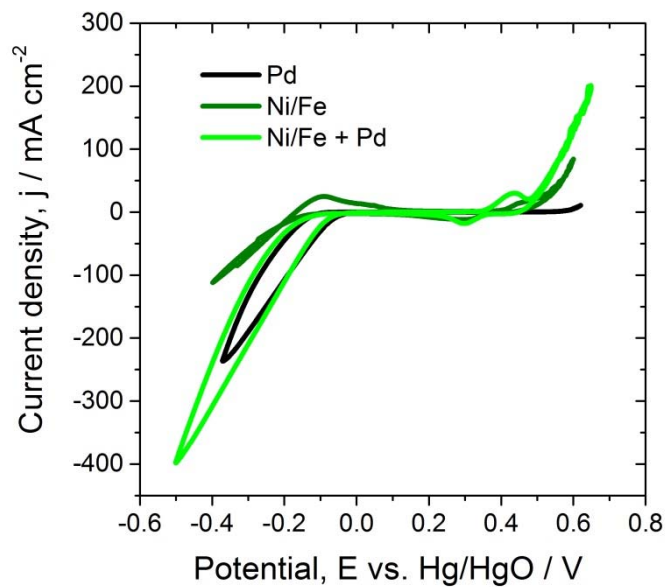
Figure 4
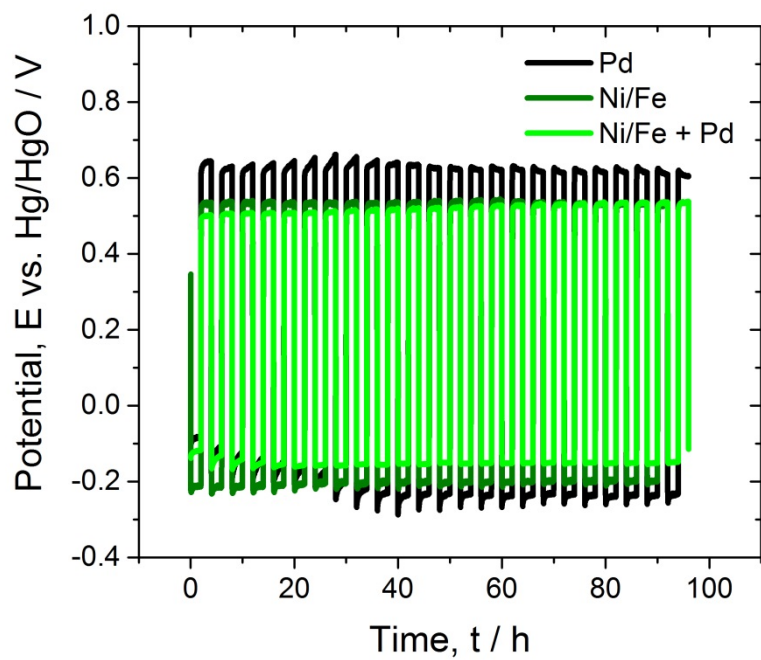
Figure 5
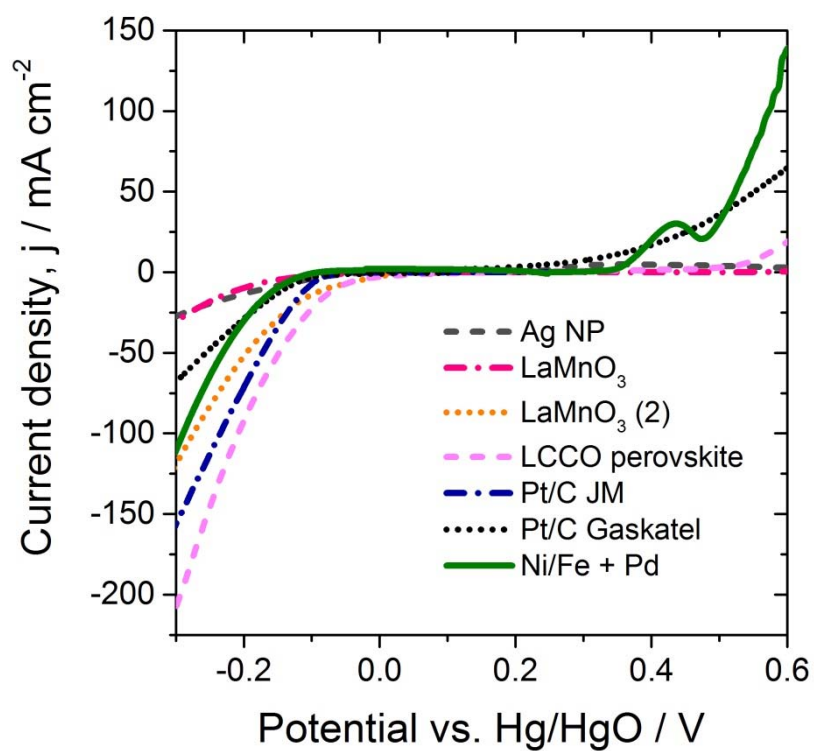
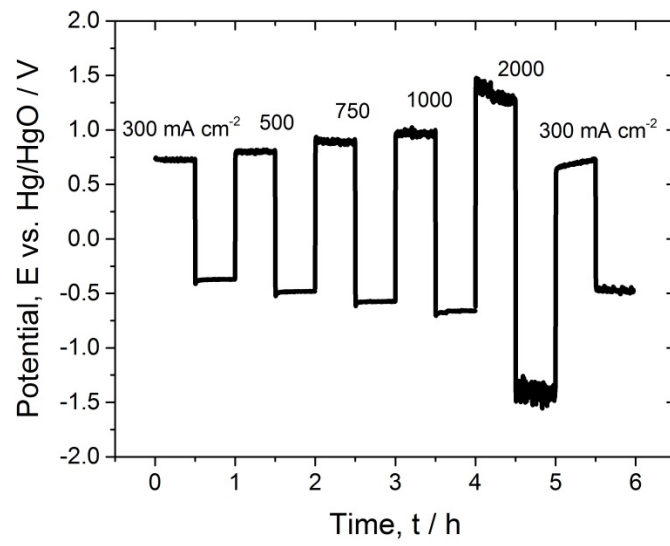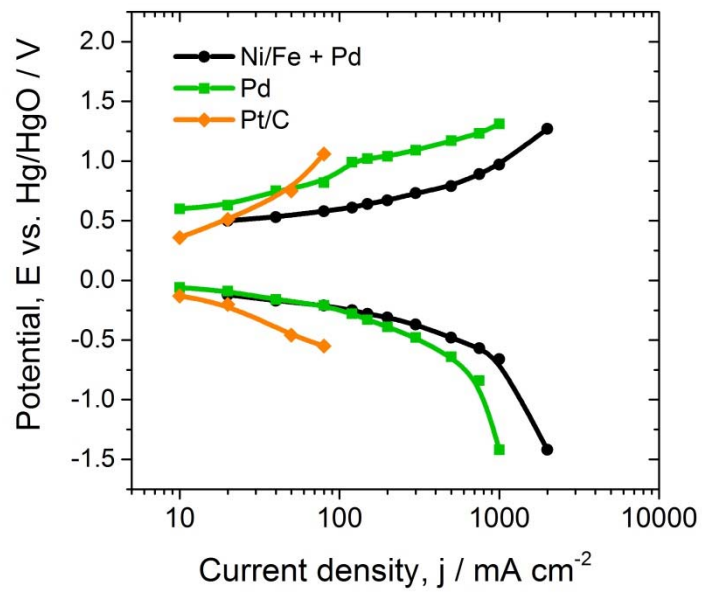**Figure 6**
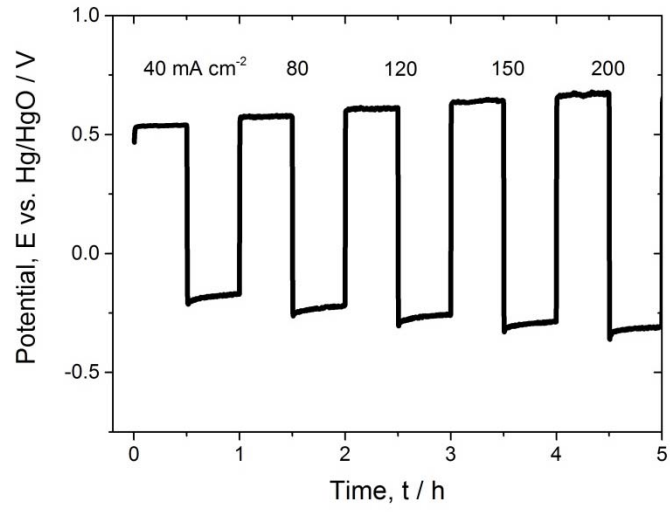
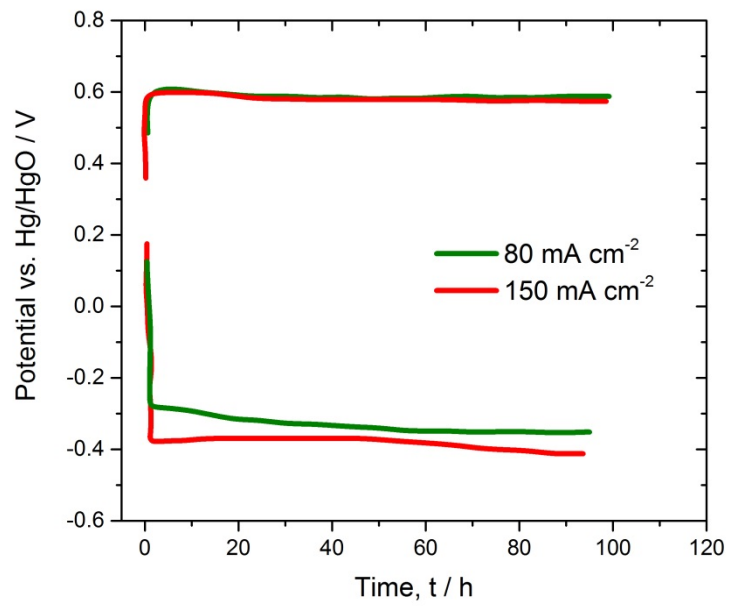**Figure 7**

Figure 8

Figure 9

Figure 10

References

1.   Y-C Lee, P-Y Peng, W-S Chang, C-M Huang. Hierarchical meso-macroporous $LaMnO_3$ electrode material for rechargeable zinc–air batteries. J. Taiwan Inst Chem Eng. 45 (2014) 2334.

2.   Z.Q. Peng, S.A. Freunberger, Y.H. Chen, P.G. Bruce. A reversible and higher-rate Li-O_2 battery. Science, 337 (2012) 563.

3.   K. Hayashi, K. Shima, F. Sugiyama. A mixed aqueous/aprotic sodium/air cell using a NASICON ceramic separator. J Electrochem Soc. 160 (2013) A1467.

4.   X. Ren, Y. Wu. A Low-overpotential potassium–oxygen battery based on potassium superoxide. J Am Chem Soc. 135 (2013) 2923.

5.   R.P. Hamlen, E.C. Jerabek, J.C. Ruzzo, E.G. Siwek. Anodes for refuelable magnesium-air batteries. J Electrochem Soc. 116 (1969) 1588.

6.   N.U. Pujare, K.W. Semkow, A.F. Sammells. A calcium oxygen secondary battery. J Electrochem Soc. 135 (1988) 260.

7.   D.R. Egan, C. Ponce de León, R.J.K. Wood, R.L. Jones, K.R. Stokes, F.C. Walsh. Developments in electrode materials and electrolytes for aluminium–air batteries. J. Power Sources, 236 (2013) 293-310.

8.   Cohn G, Starosvetsky D, Hagiwara R, Macdonald DD, Ein-Eli Y. Silicon-air batteries. Electrochem Comm. 11 (2009) 1916.

9.   R.D. McKerracher, C. Alegre, V. Baglio, A.S. Aricò, C. Ponce de León, F. Mornaghini, M. Rodlert, F.C. Walsh. A nanostructured functional Pd/C gas-diffusion electrode for metal-air batteries. Electrochim. Acta, 174 (2015) 508-515.

10.   L. Öjefors, L. Carlsson. An iron-air vehicle battery. J. Power Sources 2 (1977/78) 287-296.

11.   Z.Y. Liu, J.L. Zhang, P.T. Yu, J.X. Zhang, R. Makharia, K.L. More, E.A. Stach, Transmission electron microscopy observation of corrosion behaviors of platinized carbon blacks under thermal and electrochemical conditions. J. Electrochem Soc. 157 (2010) B906-B913.

12.   X. Li, D. Pletcher, A.E. Russell, F.C. Walsh, R.G.A. Wills , S.F. Gorman, S.W.T. Price, S.J. Thompson. A novel bifunctional oxygen GDE for alkaline secondary batteries. Electrochem. Comm. 34 (2013) 228-230.

13.   A. Ikezawa, K. Miyazaki, T. Fukutsuka, T. Abe, J. Electrochem. Soc. 162 (2015) A1646-A1653.

14. Z. Shuxin, H. Chenghuan, H. Kelong, X. Tu, F.H. Hongxia, Preparation of homogeneous nanoporous $La_{0.6}Ca_{0.4}CoO_3$ for bi-functional catalysis in an alkaline electrolyte, Electrochem. Comm. 13(4) (2011) 321-324.

15. D. Pletcher, X. Li, S.W.T. Price, A.E. Russell, T. Sönmez, S. J. Thompson, Comparison of the Spinels Co_3O_4 and $NiCo_2O_4$ as Bifunctional Oxygen Catalysts in Alkaline Media, Electrochima Acta 188 (2016) 286-293.

16. X. Li, D. Pletcher, A.E. Russell, F.C. Walsh, RG.A. Wills, S.F. Gorman, S.W.T. Price, S.J. Thompson. A novel bifunctional oxygen GDE for alkaline secondary batteries, Electrochem Comm. 34 (2013) 228-230.

17. J. Prakash, D. A. Tryk, E. B. Yeager, Kinetic Investigations of Oxygen Reduction and Evolution Reactions on Lead Ruthenate Catalysts, J. Electrochem. Soc. 146 (1999) 4145-4151.

18. S.Velraj, J.H. Zhu. Cycle life limit of carbon-based electrodes for rechargeable metal-air battery application. J. Electroanal. Chem. 736 (2015) 736.

19. M. De Koninck, P. Manseau, B. Marsan. Preparation and characterization of Nb-doped TiO_2 nanoparticles used as a conductive support for bifunctional $CuCo_2O_4$ electrocatalyst. J. of Electroanal. Chem. 611 (2007) 67.

20. O. Kasian, T. Luk'yanenko, A. Velichenko, R. Amadelli, Electrochemical behavior of platinized Ebonex® electrodes. Int. J. Electrochem. Sci. 7 (2012) 7915-7926.

21. Y. Shimizu, H. Matsuda, N. Miura, N. Yamazoe. Bifunctional oxygen electrode using large surface area Perovskite-type oxide catalyst for rechargeable metal-air batteries. Chem. Let. 6 (1992) 1033.

22. A. Stassi, I. Gatto, V. Baglio, A.S. Aricò. Evaluation of palladium-based electrocatalyst for oxygen reduction and hydrogen oxidation in intermediate temperature polymer electrolyte fuel cells. Int. J. Hydrogen Energy, 39 (2014) 21581-21587.

23. A.S. Aricò, V. Baglio, A. Di Blasi, E. Modica, P.L. Antonucci, V.J. Antonucci, Analysis of the high-temperature methanol oxidation behaviour at carbon-supported Pt–Ru catalysts. Electroanal. Chem., 557 (2003) 167-176.

24. W.A. Steen, S.W. Han, Q. Yu, R.A. Gordon, J.O. Cross, E.A. Stern, G.T. Seidler, K.M. Jeerage, D.T. Schwartz, Structure of Cathodically Deposited Nickel Hexacyanoferrate Thin Films Using XRD and EXAFS, Langmuir 18 (2002) 7714-7721.

25. S.N. Ghosh, Infrared spectra of the Prussian blue analogues, J. Inorg.Nucl.Chem., 36 (1974) 2465-2466.

26. I.M. Ismail, M.R. El-Sourougy, N. Abdel Moneim, H.F. Aly, Preparation, characterization, and utilization of potassium nickel hexacyanoferrate for the

separation of cesium and cobalt from contaminated waste water, Journal of Radioanalytical and Nuclear Chemistry, 237 (1998) 97-103.

27. L. Hu, P. Zhang, Q. Chen. J. Mei, N. Yan, Room-temperature synthesis of Prussian blue analogue $Co_3[Co(CN)_6]_2$ porous nanostructures and their CO_2 storage properties, RSC Adv. 1 (2011) 1574-1578. 10.1039/C1RA00624J

28. D.M. Gil, M. Avila, E. Reguera, S. Pagola, M.I. Gomez, R.E. Carbonio, Lead hexacyanoferrate(II) tetrahydrate: Crystal structure, FTIR spectroscopy and thermal decomposition studies, Polyhedron, 33 (2012) 450-455.

29. C. Song, J. Zhang, Electrocatalytic oxygen reduction reaction, PEM fuel cell electrocatalysts and catalyst layers, fundamentals and applications, J. Zhang (Ed.) (2008) Vol. XXI, ISBN: 978-1-84800-935-6, pp. 89-129.

30. K. Kinoshita, Electrochemical oxygen technology, Wiley, New York, 1992.

31. J.P. Meyers, R.M. Darling, Model of carbon corrosion in PEM fuel cells, J. Electrochem. Soc. 153 (2006) A1432-A1442.

32. R.D. McKerracher, C. Ponce de Léon, R.G.A. Wills, A.A. Shah, F.C. Walsh, A review of the iron-air secondary battery for energy storage, ChemPlusChem 80 (2015) 323–335.

33. S. Zhang, H. Zhang., S. Liu, F. Tu, W. Zhang, C. Zhao, Optimized Perovskite Electrocatalyst for bifunctional air electrode by impedance spectroscopy analysis. Int. J. Electrochem. Sci 9 (2014) 1690-1701.

34. M. Yuasa, M. Nishida, T. Kida, N. Yamazoe, K. Shimanoe. Bi-functional oxygen electrodes using $LaMnO_3/LaNiO_3$ for rechargeable metal-air batteries. J. Electrochem. 158 (2011) A605-A610.

35. C. Zhu, A. Nobuta, I. Makatsugawa, T. Akiyama, Solution combustion synthesis of $LaMO_3$ (M = Fe, Co, Mn) perovskite nanoparticles and the measurement of their electrocatalytic properties for air cathode Int. J. Hydrogen Energy 38 (2013) 13238-13248.

36. N. Sasikala, K. Ramya, K.S. Dhathathreyan, Bifunctional electrocatalyst for oxygen/air electrodes. Energy Conversion and Management 77 (2014) 545-549.

37. D.E. Pissinis, L.E. Sereno, J.M. Marioli, Utilization of special potential scan programs for cyclic voltammetric development of different nickel oxide-hydroxide species on Ni based electrodes, Open J. Phys. Chem. 2 (2012) 23-33.